ChemComm

COMMUNICATION

View Article Online
View Journal | View Issue

Check for updates

Cite this: *Chem. Commun.*, 2022, 58, 9417

Received 16th March 2022,
Accepted 18th July 2022

DOI: 10.1039/d2cc01507b

rsc.li/chemcomm

Open Access Article. Published on 18 July 2022. Downloaded on 7/30/2025 3:36:28 PM.
This article is licensed under a Creative Commons Attribution 3.0 Unported Licence.

pH-Dependent fluorescence of $[La(OH)_2]^+[ARS]^-$ hybrid nanoparticles for intracellular pH-sensing†

Kristina Sabljo,[a] Joanna Napp,[bc] Frauke Alves *[bc] and Claus Feldmann *[a]

Saline inorganic–organic hybrid nanoparticles (IOH-NPs) $[La(OH)_2]^+[ARS]^-$ (ARS: alizarin red S) are prepared in water as a new compound (particle size: 47 ± 7 nm, ARS load: 65 wt%). The IOH-NPs not only show a pH-dependent absorption colour but also a pH-dependent fluorescence with green emission at pH 5.0–9.0 and red emission at pH < 4.5. According to first *in vitro* studies, the pH-dependend fluorescence can be used to monitor nanoparticle internalization in cells as well as the respective intracellular pH.

The pH value is one of the fundamental parameters to characterize biological systems.[1] Monitoring changes of the pH is most relevant to study the cell-cycle phase (*e.g.*, growth, division) or cellular internalization processes (*e.g.*, phagocytosis, endocytosis, receptor-ligand internalization).[2] Due to different metabolic pathways, the pH level can also allow to differentiate cell compartments from each other (*e.g.*, endosomes, lysosomes).[3] Unusual changes of the intracellular pH (pH_i), and specifically acidic pH levels, can point to inappropriate cell functions and were reported to indicate apoptosis and necrosis or diseases such as Alzheimer's[4] or cancer.[5] Moreover, a disturbed pH_i and pH_i-homeostasis contribute to essentially all hallmarks of cancer.[6] Thus, the pH_i can provide manifold information about physiological and pathological processes.

To monitor the pH of biological systems, pH-sensitive fluorescent probes seem most promising and offer several advantages in comparison to other pH-sensing techniques, such as absorbance spectroscopy, microelectrodes, or nuclear magnetic resonance (NMR).[7] Genereally, fluorescent probes allow for high spatial and temporal resolution as well as high sensitivity. Moreover, optical imaging is often non-invasive to cells, tissue and living beings.[8] For this purpose, different nanoparticle-based systems were suggested, including quantum dots, carbon and silica nanoparticles, or nanosized polymers and metal–organic frameworks.[9] Such nanoparticle systems have several advantages over molecular probes, including higher local brightness, higher photostability, higher sensitivity, and easier functionalization. However, current drawbacks include a limited pH range (usually covering not more than 3–4 units), a less sensitive change of the fluorescence intensity as response, the complexity of composition and structure, and/or the toxicity of the one or other ingredient of the fluorescent probe.[9a]

Aiming at nanomaterials for drug delivery and multimodal imaging, we have developed the concept of inorganic–organic hybrid nanoparticles (IOH-NPs).[10] This concept is characterized by saline compounds, consisting of an inorganic cation and a functional organic anion. The functional organic anion can be a drug and/or a fluorescent dye, which contains phosphate, sulfonate, or carboxylate groups. Together with a suitable cation, this functional organic anion forms an insoluble saline compound in water. Specific examples, for instance, include $[ZrO]^{2+}[FMN]^{2-}$, $[Gd(OH)]^{2+}[NFR]^{2-}$, $[ZrO]^{2+}[DUT]^{2-}$, or $[GdO]^+[ICG]^-$ (FMN: flavinmononucleotide, NFR: nuclear fast red, DUT: Dyomics-647 uridine triphosphate, ICG: indocyanine green) showing green, red, or (near-)infrared emission.[11] These IOH-NPs are characterized by aqueous synthesis, unprecedented dye load (70–85 wt% of total nanoparticle weight), and intense emission. With $[La(OH)_2]^+[ARS]^-$, we here show IOH-NPs with a pH-sensitive fluoresence for the first time. Herein, lanthanum (La^{3+}) as inorganic cation is combined with the pH indicator alizarin red S (1,2-dihydroxy-9,10-anthraquinone-sulfonicacid, ARS) as functional organic anion (Fig. 1). The anthraquinone dye ARS is used in textile industries, but also as histochemical reagent, and pH indicator.[12] For the first time, we here show a pH-dependent emission of ARS, the characterization of $[La(OH)_2]^+[ARS]^-$ IOH-NPs, and their use as

[a] *Karlsruhe Institute of Technology (KIT), Institute for Inorganic Chemistry, Engesserstrasse 15, 76131, Karlsruhe, Germany. E-mail: claus.feldmann@kit.edu*
[b] *University Medical Center Goettingen (UMG), Institute for Diagnostic and Interventional Radiology, Robert Koch Str. 40, 37075, Goettingen, Germany. E-mail: falves@gwdg.de*
[c] *Max Planck Institute for Multidisciplinary Sciences, Translational Molecular Imaging, Hermann-Rein-Strasse 3, 37075, Goettingen, Germany*

† Electronic supplementary information (ESI) available: Details related to the analytical methods, experimental, pH-dependent behaviour of Na(ARS), material characterization of $[La(OH)_2]^+[ARS]^-$ IOH-NPs, and *in vitro* studies. See DOI: https://doi.org/10.1039/d2cc01507b

Open Access Article. Published on 18 July 2022. Downloaded on 7/30/2025 3:36:28 PM.
This article is licensed under a Creative Commons Attribution 3.0 Unported Licence.

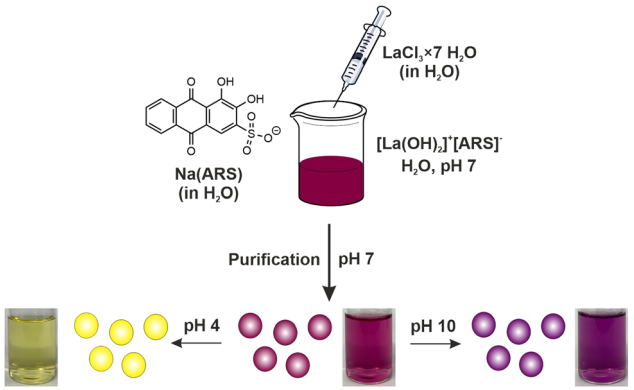

Fig. 1 Scheme illustrating the aqueous synthesis of $[La(OH)_2]^+[ARS]^-$ IOH-NPs and photos showing the colour of suspensions at different pH values.

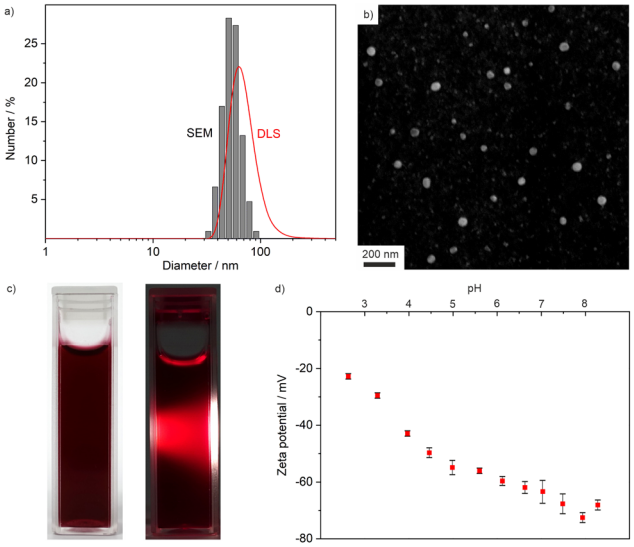

Fig. 2 Particle size of $[La(OH)_2]^+[ARS]^-$ IOH-NPs: (a) particle size distribution according to DLS (in water) and statistical evaluation of >100 particles on SEM images; (b) SEM images; (c) photos of aqueous IOH-NP suspensions in daylight and with Tyndall cone; (d) zeta potential of aqueous IOH-NP suspension.

pH-sensitive nanoprobe, including first *in vitro* studies as a proof-of-concept.

The synthesis of $[La(OH)_2]^+[ARS]^-$ IOH-NPs is characterized by a straightforward water-based precipitation reaction at room temperature (Fig. 1). Accordingly, a concentrated aqueous solution of $LaCl_3{\cdot}7H_2O$ was injected with vigorous stirring into an aqueous solution of Na(ARS). Following the La Mer–Dinegar model of particle nucleation and particle growth,[13] a high supersaturation was induced by the injection, which causes a rapid particle nucleation, and thus, the formation of small-sized nanoparticles. After purification, a pink suspension of $[La(OH)_2]^+[ARS]^-$ IOH-NPs was obtained at pH 7 (Fig. 1). Upon variation of the pH value, the $[La(OH)_2]^+[ARS]^-$ IOH-NP suspensions indeed show a pH-dependent colour change, which is – as expected – similar to solutions of the freely dissolved ARS indicator (ESI:† Fig. S1).[14] Accordingly, the colour of aqueous suspensions turned from pink to yellow when decreasing the pH from 7 to 4 (Fig. 1). Moreover, the colour of suspensions turned from pink to violet when increasing the pH from 7 to 10.

According to dynamic light scattering (DLS), aqueous suspensions of the as-prepared $[La(OH)_2]^+[ARS]^-$ IOH-NPs exhibit a mean hydrodynamic diameter of 69 ± 15 nm (Fig. 2a and c). Scanning electron microscopy (SEM) confirms the presence of uniform spherical particles with a mean diameter of 47 ± 7 nm (Fig. 2a and b). This value was calculated by statistical evaluation of >100 particles. The larger particle diameter obtained from DLS reflects the hydrodynamic diameter and the presence of a rigid layer of adsorbed water molecules on the particle surface.[15] The realization of uniform nanoparticles immediately after synthesis without the need for any additional surface-active agent for size control and colloidal stabilization is noteworthy and can be ascribed to an intrinsic charge stabilization as indicated by the zeta potential of the as-prepared IOH-NPs. $[La(OH)_2]^+[ARS]^-$ shows negative charging of −40 to −65 mV in water in the physiologically relevant pH range of 5–8 (Fig. 2d). According to DLS and SEM, particle size and shape of the IOH-NPs remain stable in a pH range of 4–8 (ESI:† Fig. S2 and S3). At strongly acidic (pH < 4) or basic (pH > 8) conditions, the particle size decreases, which indicates beginning particle dissolution. To prove the chemical composition of the $[La(OH)_2]^+[ARS]^-$ IOH-NPs, different analytical methods were used including X-ray diffraction, Fourier-transformed infrared spectroscopy, energy-dispersive X-ray spectroscopy, elemental analysis, and thermogravimetry (ESI:† Fig. S4–S7). Taken together, they confirm the composition $[La(OH)_2]^+[ARS]^-$ with 65 wt% ARS of total IOH-NP mass.

Aiming at tumour diagnosis, optical imaging is generally a very promising option due to the use of harmless irradiation, low costs, and potentially high spatial and temporal resolution with high sensitivity.[16] In comparison to healthy tissue – normally with a pH of about 7.4 – the pH of the tumour microenvironment by extracellular acidification ranges at 6.2–6.9.[1,5] In cancer cells, concomitant intracellular alkalization of the cytoplasm results in a constitutively increased pH_i that is higher than the external pH. This "reversed" pH gradient is thought to be permissive for some of the acquired characteristics of cancers.[5,6] Moreover, the pH of the lysosomal lumen of cancer cells with 4.5 to 5.5 can be significantly lower than the pH of normal cells (pH 5.0–6.0).[5,14] Here, a suitable emissive nanoprobe that allows to indicate such acidic pH ranges is highly desirable and could allow to monitor cancer *via* fluorescence detection.

The pH-indicator ARS is generally known to change its absorption both in the acidic range (pK_a = 5.5) and in the basic range (pK_a = 10.8).[17] To evaluate the pH-dependent properties of the $[La(OH)_2]^+[ARS]^-$ IOH-NPs, first of all, the absorption of the nanoparticle suspension was examined and compared to solutions of freely dissolved ARS (Fig. 3; ESI:† Fig. S1). Accordingly, the IOH-NPs show a considerable colour shift from pink (pH = 5.0–9.0) to violet (pH > 9.0), and most important to pale yellow (pH < 4.5) (Fig. 3a). To quantify the visible absorption,

 This journal is © The Royal Society of Chemistry 2022

Open Access Article. Published on 18 July 2022. Downloaded on 7/30/2025 3:36:28 PM.
This article is licensed under a Creative Commons Attribution 3.0 Unported Licence.

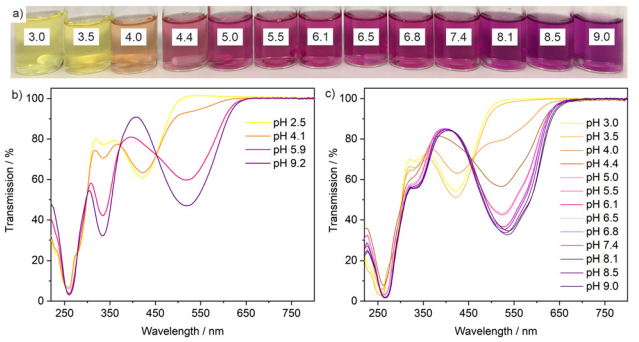

Fig. 3 Optical properties of the as-prepared $[La(OH)_2]^+[ARS]^-$ IOH-NPs at different pH values: (a) photos of aqueous IOH-NP suspensions (0.05 μmol mL^{-1}) at different pH values, (b) UV-vis spectra of Na(ARS) (aqueous solutions, 0.05 μmol mL^{-1}), (c) UV-vis spectra of $[La(OH)_2]^+[ARS]^-$ IOH-NPs (aqueous suspensions, 0.05 μmol mL^{-1}).

UV-vis spectra were recorded at four different pH values, *i.e.*, 2.5, 4.1, 5.9, and 9.2 (Fig. 3b). Thus, the IOH-NPs show a shift of the absorption maximum at 530 nm (pH 9.0 to 4.5) to 420 nm (pH $<$ 4.5). This pH-dependent shift of the optical absorption is in accordance with solutions of freely dissolved ARS and can be related to its molecular structure with two deprotonated OH groups (pH $>$ 10.8) *via* one deprotonated OH group (pH 5.0 to 10.8) to totally protonated OH groups (pH $<$ 5.5, ESI:† Fig. S1b).[17]

Even more interesting than the pH-dependent absorption is the question regarding a pH-dependent emission of the $[La(OH)_2]^+[ARS]^-$ IOH-NPs. To the best of our knowledge, a pH-dependent fluorescence of ARS has not been reported until now. In fact, the emission of freely dissolved ARS in water is weak. For the $[La(OH)_2]^+[ARS]^-$ IOH-NPs with its high concentration of ARS per nanoparticle volume, however, fluorescence spectroscopy indeed shows good fluorescence at 550–600 nm (Fig. 4) upon excitation at 300–500 nm (Fig. 4a). Even more surprising is the observation of a pH-dependent shift of the emission (Fig. 4b). Thus, the green emission (550–600 nm) observed at pH 5.0 to 9.0 shifts to a red emission (550–700 nm) at acidic pH ($<$4.5). In sum, the novel $[La(OH)_2]^+[ARS]^-$ IOH-NPs indeed show the intended pH-dependent emission. Due to the high ARS-load of the IOH-NPs (65 wt%), intense emission is observed, which can be detected even by the naked eye.

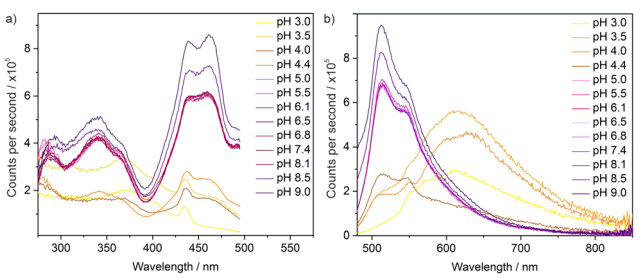

Fig. 4 Fluorescence of the as-prepared $[La(OH)_2]^+[ARS]^-$ IOH-NPs at different pH values: (a) excitation spectra (λ_{em}: 512 nm); (b) emission spectra (λ_{exc}: 462 nm).

The pH-dependent emission of the $[La(OH)_2]^+[ARS]^-$ IOH-NPs can be of particular interest for biomedical studies, first of all, to visualize the intracellular pH (pH_i) and, on the longer term, to monitor tumours and eventually metastasis. As a very first prove-of-the-concept, *in vitro* studies were initiated. Accordingly, MH-S macrophages were incubated (up to 5 h at 25 °C) with $[La(OH)_2]^+[ARS]^-$ suspensions (up to 50 μL mL^{-1}). MTT assays indicate a low toxicity of the $[La(OH)_2]^+[ARS]^-$ IOH-NPs (ESI:† Fig. S8). Accordingly, MH-S macrophages were incubated (up to 5 h at 25 °C) with $[La(OH)_2]^+[ARS]^-$ suspensions (50 μg mL^{-1}). Already after 30 min of incubation, a successful cellular uptake of the IOH-NPs is clearly indicated by intense green emission at 500–550 nm (Fig. 5). Furthermore, weak emission also occurs at 550–650 nm and 650–750 nm. The emission clearly indicates successful cell uptake with the IOH-NPs located in endosomes (Fig. 5a). After 5 hours, the type of emission is shifted and now shows dominating red (550–650 nm) and near-infrared emission (650–750 nm, Fig. 5b). Based on an endocytic pathway, the internalized IOH-NPs encounter a successively decreasing pH in early endosomes, late endosomes, and lysosomes. Acidification facilitates, among other processes, the dissociation of receptor ligands (pH ~ 6.2) and enables a selective activation of the lysosomal hydrolase (pH ~ 4.5–5.2).[18] Here, we show that a low pH within the late endosomes can be successfully determined by the $[La(OH)_2]^+[ARS]^-$ IOH-NPs (Fig. 5b), which was confirmed by the observation that these internalized IOH-NPs localized with Rab7, a marker of late endosomes (Fig. 6). IOH-NPs do not co-localize with Rab11, which is associated with recycling endosomes (ESI:† Fig. S9). Altogether, the observed pH-dependent emission of the IOH-NPs *in vitro* is similar to the

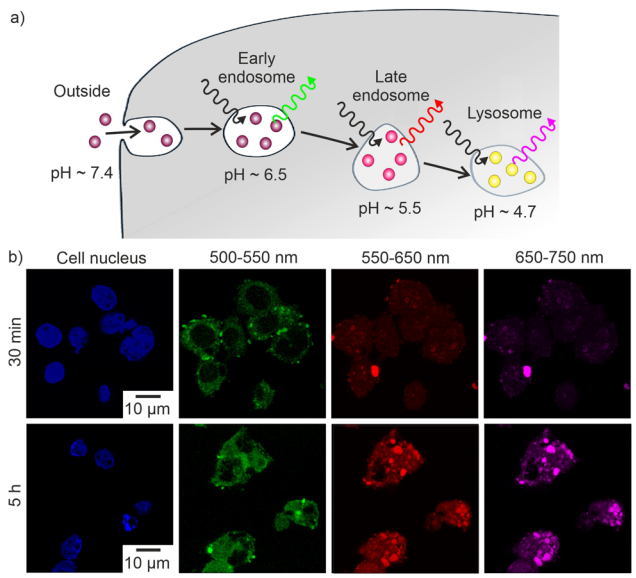

Fig. 5 *In vitro* life-cell imaging study of cell uptake of $[La(OH)_2]^+[ARS]^-$ IOH-NPs: (a) scheme of temporal sequence of IOH-NP uptake with pH-dependent fluorescence; (b) fluorescence images of murine MHS macrophages 30 min and 5 h after cultivation with $[La(OH)_2]^+[ARS]^-$ IOH-NPs (50 μL mL^{-1}) acquired by different fluorescent emission spectra (cell nuclei show blue emission due to 4′,6-diamidin-2-phenylindole (DAPI) staining).

Open Access Article. Published on 18 July 2022. Downloaded on 7/30/2025 3:36:28 PM.
This article is licensed under a Creative Commons Attribution 3.0 Unported Licence.

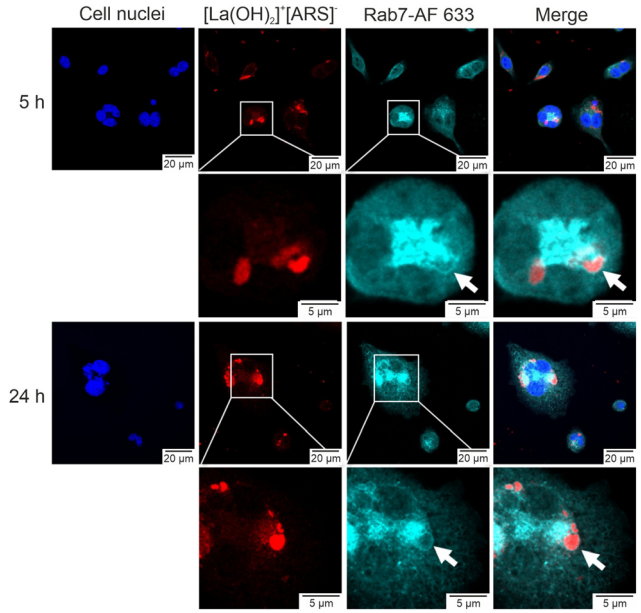

Fig. 6 $[La(OH)_2]^+[ARS]^-$ IOH-NPs co-localize with late endosomes: MH-S cells were incubated with the IOH-NPs (red) for 5 h or 24 h and fixed. Staining was performed with an anti-Rab7-antibody followed by the Alexa Fluor 633 (AF 633) conjugated secondary antibody (cyan blue) as indicated by the arrow. Nuclei were labelled with Hoechst 33342 (dark blue). Second and lowest panel show magnifications of the selected ROIs shown in the first and third panel. Right panels show merged images.

fluorescence observed in aqueous suspensions and confirms the feasibility of $[La(OH)_2]^+[ARS]^-$ for biomedical studies.

In conclusion, $[La(OH)_2]^+[ARS]^-$ IOH-NPs with pH-dependent fluorescence are shown for the first time. The IOH-NPs are prepared *via* straightforward aqueous synthesis and contain the pH indicator ARS (alizarin red S) with a load of 65 wt%. They exhibit a mean particle size of 47 ± 7 nm and are chemically and colloidally highly stable at pH 4–8. $[La(OH)_2]^+[ARS]^-$ shows the expected absorption colour shift from pink (pH = 5.0–9.0) to yellow (pH $<$ 4.5). The fluorescence and a pH-dependent fluorescence shift are observed for the first time and result in a green emission at pH 5.0–9.0 and a red emission at pH $<$ 4.5. Due to the high ARS-load per nanoparticle, both the absorptive as well as the emissive colour change are easy to detect. Beside the spectroscopic characterization of the pH-dependent absorption and emission of the new compound, first *in vitro* studies show the temporal cell uptake of the IOH-NPs in endosomes. The temporal pH shift from 7.4 to 4.7 is again accommpanied with a fluorescence shift from green to red. Based on this proof-of-the-concept study, the novel $[La(OH)_2]^+[ARS]^-$ IOH-NPs can become very interesting as easy-to-prepare fluorescent pH nanoprobes to monitor the viability of biological systems, including metabolic pathways, cell-cycle phases, pH homeostasis of tumours, apoptosis, and necrosis.

The authors thank the Deutsche Forschungsgemeinschaft (DFG) for funding (SinDrug: FE 911/13-1 and NA 1313/2-1).

Conflicts of interest

There are not conflicts to declare.

Notes and references

1 A. Roos and W. F. Boron, *Physiol. Rev.*, 1981, **61**, 296–434.
2 (*a*) M. Miksa, H. Komura, R. Wu, K. G. Shah and P. J. Wang, *J. Immunol. Methods*, 2009, **342**, 71–77; (*b*) M. Lakadamyali, M. J. Rust, H. P. Babcock and X. Zhuang, *Proc. Natl. Acad. Sci. U. S. A.*, 2003, **100**, 9280–9285; (*c*) E. J. Adie, S. Klinka, L. Smith, M. J. Francis, A. Marenghi, M. E. Cooper, M. Briggs, N. P. Michaels, G. Milligan and S. Game, *Biotechniques*, 2002, **33**, 1152–1156.
3 J. R. Casey, S. Grinstein and J. Orlowski, *Nat. Rev. Mol. Cell Biol.*, 2010, **11**, 50–61.
4 T. A. Davies, R. E. Fine, R. J. Johnson, C. A. Levesue, W. H. Rathbun, K. F. Seetoo, S. J. Smith, G. Strohmeier, L. Volicer, L. Delva and E. R. Simons, *Biochem. Biophys. Res. Commun.*, 1993, **194**, 537–543.
5 B. A. Webb, M. Chimenti, M. P. Jocobson and D. L. Barber, *Nat. Rev. Cancer*, 2011, **11**, 671–677.
6 S. F. Pedersen, I. Novak, F. Alves, A. Schwab and L. A. Pardo, *BioEssays*, 2017, **39**, 160025.
7 J. Srivastava, D. L. Barber and M. P. Jacobson, *Physiology*, 2007, **22**, 30–39.
8 J. Han and K. Burgees, *Chem. Rev.*, 2010, **110**, 2709–2728.
9 (*a*) T. F. Abelha, C. A. Dreiss, M. A. Green and L. A. Dailey, *J. Mater. Chem. B*, 2020, **8**, 592–606; (*b*) M. Shamsipur, A. Barati and Z. Nematifar, *J. Photochem. Photobiol., C*, 2019, **39**, 76–141; (*c*) J.-T. Hou, W. X. Ren, K. Li, J. Seo, A. Sharma, X.-Q. Yu and J. S. Kim, *Chem. Soc. Rev.*, 2017, **46**, 2076–2090; (*d*) B. Chu, H. Wang, B. Song, F. Peng, Y. Su and Y. He, *Anal. Chem.*, 2016, **88**, 9235–9242; (*e*) J. Huang, L. Ying, X. Yang, Y. Yang, K. Quan, H. Wang, N. Xie, M. Ou, Q. Zhou and K. Wang, *Anal. Chem.*, 2015, **87**, 8724–8731; (*f*) W. Shi, X. Li and H. Ma, *Methods Appl. Fluoresc.*, 2014, **2**, 042001; (*g*) L. Wang and C. Li, *J. Mater. Chem.*, 2011, **21**, 15862–15871.
10 (*a*) J. G. Heck, J. Napp, S. Simonato, J. Möllmer, M. Lange, H. R. Reichardt, R. Staudt, F. Alves and C. Feldmann, *J. Am. Chem. Soc.*, 2015, **137**, 7329–7336; (*b*) B. L. Neumeier, M. Khorenko, F. Alves, O. Goldmann, J. Napp, U. Schepers, H. M. Reichard and C. Feldmann, *ChemNanoMat*, 2019, **5**, 24–45.
11 (*a*) M. Poß, E. Zittel, A. Meschkov, U. Schepers and C. Feldmann, *Bioconjugate Chem.*, 2018, **29**, 2818–2828; (*b*) J. Napp, M. A. Markus, J. G. Heck, C. Dullin, W. Möbius, D. Gorpas, C. Feldmann and F. Alves, *Theranostics*, 2018, **8**, 6367–6368; (*c*) M. Poß, R. J. Tower, J. Napp, L. C. Appold, T. Lammers, F. Alves, C.-C. Glüer, S. Boretius and C. Feldmann, *Chem. Mater.*, 2017, **29**, 3547–3554.
12 (*a*) E. Gurr, *Synthetic Dyes in Biology, Medicine and Chemistry*, Academic Press; London, 1971, p. 234–235; (*b*) M. A. Khosa, S. S. Shah and M. F. Nazar, *J. Dispersion Sci. Technol.*, 2011, **32**, 1634–1640.
13 V. K. LaMer and R. H. J. Dinegar, *J. Am. Chem. Soc.*, 1950, **72**, 4847–4854.
14 K. Glunde, S. E. Guggino, M. Solaiyappan, A. P. Pathak, Y. Ichikawa and Z. M. Bhujwalla, *Neoplasia*, 2003, **5**, 533–545.
15 R. Witter, M. Roming, C. Feldmann and A. S. Ulrich, *J. Colloid Interface Sci.*, 2013, **390**, 250–257.
16 (*a*) S. Kunjachan, J. Ehling, G. Storm, F. Kiessling and T. Lammers, *Chem. Rev.*, 2015, **115**, 10907–10937; (*b*) T. L. Doane and C. Burda, *Chem. Soc. Rev.*, 2012, **41**, 2885–2911.
17 A. A. Shalaby and A. A. Mohamed, *RSC Adv.*, 2020, **10**, 11311–11316.
18 (*a*) M. A. Khosa, S. S. Shah and M. F. Nazar, *J. Dispersion Sci. Technol.*, 2011, **32**, 1634–1640; (*b*) S. Mukherjee, R. N. Ghosh and F. R. Maxfield, *Phys. Rev.*, 1997, 77, 759–803.

This journal is © The Royal Society of Chemistry 2022